 doi:10.20944/preprints201806.0174.v1

Type of the Paper (Review)

Computing the Effect of Environmental Damage on Aircraft Structural Integrity

Rhys Jones [1,*], Daren Peng [2] and Neil Matthews [3] ,Nam Phan[4]

[1] Centre of Expertise for Structural Mechanics, Department of Mechanical and Aerospace Engineering, Monash University, Clayton, Victoria, 3800, Australia ; rhys.jones@monash.edu
[2] Centre of Expertise for Structural Mechanics, Department of Mechanical and Aerospace Engineering, Monash University, Clayton, Victoria, 3800, Australia; rhys.jones@monash.edu
[3] RUAG Australia, 836 Mountain Highway, Bayswater, VIC 315, Australia; Neil.Matthews@ruag.com
[4] Structures Division, Naval Air Systems Command, Patuxent River, MD 20670, United States; nam.phan@navy.mil
* Correspondence: rhys.jones@monash.edu; Tel.: +61-48-775-3232

Abstract: This paper studies the combined effect of corrosion and fatigue on the growth of cracks in aircraft and on the effect of skin corrosion and stress corrosion cracking on the load bearing capacity of rib stiffened aircraft wings. In this context it is shown that the growth of cracks from surface pitting, and also from intergranular cracking at a fastener hole, can be accurately computed using the Hartman-Schijve variant of the NASGRO crack growth equation. The examples studied support the lead crack approach, that has been independently developed by the USAF and the Australian Defence Science Technology Group, in which the growth of lead cracks is often exponential. In the case of skin corrosion it is shown that to be consistent with the US Joint Service Structural Guidelines (JSSG2006) assessment of its effect on the load bearing capacity of the wing should involve an assessment of whether at 115% DLL the remaining material exceeds the yield stress of the material.

Keywords: operational aircraft; skin corrosion; fatigue crack growth; stress corrosion cracking; buckling

1. Introduction

Despite the fact that the importance of fatigue and corrosion to engineering structures has been recognised since the mid 19th century, and despite the problems that have arisen as a result of aging aircraft [2-8], rail and civil infrastructure [9-12] the prediction of the effect of corrosion and fatigue on the operational life of a structure is still largely an empirical science. Whilst the Aloha accident [3] was the first to bring the problem of the combined effect of corrosion and fatigue to the attention of the general public it has long been known that the corrosion of steel bridges can have a marked effect on structural integrity. Indeed, the collapse of the I35W bridge in Minneapolis, USA led US Rep. Michael Conway (R-TX11) to introduce the Bridge Life Extension Act of 2008. Transportation for America subsequently conducted an analysis of the US National Bridge Inventory [12] and reported that one in nine U.S. bridges were rated as structurally deficient. In this context it should be noted that for steel bridges the primary problems essentially result from either corrosion due to exposure of the steel to atmospheric conditions and/or from small non detectable initial material discontinuities [13]. As a result the US National Cooperative Highway Research Program, NCHRP Synthesis study [13] highlighted the need to develop advanced fatigue life calculation procedures that were capable of accounting for non visible cracks in steel bridges. Indeed, the need to be able to account for small sub mm initial defects is reinforced in the US Federal Highway Administration Steel Bridge Design Handbook [14] where it was noted that crack growth essentially starts from day

Preprints (www.preprints.org) | NOT PEER-REVIEWED | Posted: 12 June 2018 doi:10.20944/preprints201806.0174.v1

one and that the majority of the life of steel bridges is consumed in growing to a size where a crack can be detected. As explained in [15] this observation coincides with that seen in the growth of cracks in operational aircraft [6, 8, 16, 17-19]. In this context it is now known [8, 16, 17-19] that the fatigue life of operational aircraft are governed by the growth of lead cracks, i.e. the fastest cracks in the structure. For aircraft "lead cracks" have the following characteristics, from [17], viz:

i. Typical initial discontinuity sizes are about equivalent to a 0.01 mm deep fatigue crack.
ii. They start to grow shortly after the aircraft is introduced into service.
iii. The majority of the life is consumed growing to a size that can be detected using existing non destructive inspection techniques.

For aircraft it has recently been shown [8, 21-24] that various independent findings [8, 21-26] support the hypothesis presented in [8, 21] that for combat and civil transport aircraft true corrosion-fatigue interaction may not occur and that the effect of the operational environment on the growth of fatigue cracks from small naturally occurring corrosion sites in combat aircraft essentially decouples with the environment:

i) Creating material discontinuities of various sizes, which depend on the level and nature of the corrosion damage, such that cracks subsequently grow from these discontinuities;
ii) Growing existing cracks/discontinuities during extended periods of inactivity.

In this paper we first explain how the Hartman-Schijve variant of the NASGRO crack growth equation [8], viz:

$$da/dN=D((\Delta K- \Delta K_{thr})/\sqrt{((1-K\_max/A))})^{\beta} \quad (1)$$

can be used to compute the effect of cracks that arise as a result of environmental damage in aircraft structures. Here D and β are constants, and A is the cyclic fracture toughness, ΔK_{thr} is defined as an apparent fatigue threshold and is dependent on crack length and R ratio. The exponent β is often approximately 2 [8, 19], see Appendix for more details.

The examples studied substantiate the lead crack approach that has been independently developed by the USAF and the Australian Defence Science Technology Group that the growth of such lead cracks is often exponential. It is also shown that what at first glance appears to anomalous crack growth data can be due to the effect of the environment on the fatigue threshold term ΔK_{thr}.

A feature about the Hartman-Schijve equation, i.e. equation (1), is that the scatter in the da/dN versus ΔK curves is captured by allowing for the variability in the term ΔK_{thr} [7, 8, 19, 20, 27, 28]. In this context it is now known [29-33] that equation (1), with the term ΔK replaced by $\Delta\sqrt{G}$ where G is the energy release rate, also holds for cracking in adhesives and delamination growth in composites and nano-composites. It is also known [30, 31] that the large scatter seen in the delamination growth curves is captured by allowing for the variability in the term $\Delta\sqrt{G}_{thr}$.

It is also shown that what at first glance appears to anomalous crack growth data can be due to the effect of the environment on the fatigue threshold term ΔK_{thr} and that, in the tests discussed, the small crack anomaly could be accounted for by allowing for changes in the threshold term ΔK_{thr}.

Having discussed the cracking from surface pitting, the interaction of cracks at fastener holes containing intergranular cracking and the ability of the Hartman-Schijve equation to help understand what appears to be anomalous crack growth data we subsequently discuss how to compute the effect of skin corrosion and stress corrosion cracking on the load bearing capacity of rib stiffened aircraft wing structures. In the case of skin corrosion it is shown that assessment of its effect on the load bearing capacity of the wing should involve an assessment of whether at 115% DLL the remaining material exceeds the yield stress of the material.

Preprints (www.preprints.org) | NOT PEER-REVIEWED | Posted: 12 June 2018 doi:10.20944/preprints201806.0174.v1

2. Crack Growth at Fastener Holes Containing Intergranular Cracking

The first problem discussed involves the effect of intergranular cracking (IGC) on crack growth in P3C Orion dome nut hole specimens (DNHS) that had intergranular corrosion (IGC) subjected to a maritime aircraft flight load spectrum [35]. A survey of the open literature suggests that the first study into the influence of multi-layer intergranular cracking (MLIGC) on crack growth was reported in [36]. In this context, the study in [36] found that crack growth at a fastener hole containing MLIGC can proceed in a fashion that was termed as 'tunnelling' in [36]. The subsequent study in [37] revealed that different levels of load transfer in MLIGC, which arose as a result of various levels of contact below the IGC surface, resulted in a similar stress concentration at the hole.

This review also reveals that, as outlined in ASTM E647-13a Appendix X3m and [15, 19, 20, 27, 38], the value of the threshold term needed to assess the effect of corrosion damage on fatigue crack growth is small so that the formulation essentially becomes a simple Paris equation with an exponent of approximately 2. As such both NASGRO and AFGROW can be used to capture the growth of cracks that emanate from small corrosion pits in operational structures.

To illustrate this consider the specimen test program discussed in [38]. The geometry of the test specimens is shown in Figure 1, from [38], and was designed so as to represent the dome nut fastener hole in a RAAF P3C Orion wing skin. The specimens were approximately 1.5 mm thick. The 6.35 mm diameter central hole contained intergranular corrosion (IGC). In these specimens the IGC occurred at different depths beneath the surface, see Figures 2 - 5 which present both the depth and location of the IGC for specimens P3-IG-33 and P3-IG-16. The test data presented in [38] was taken from [39].

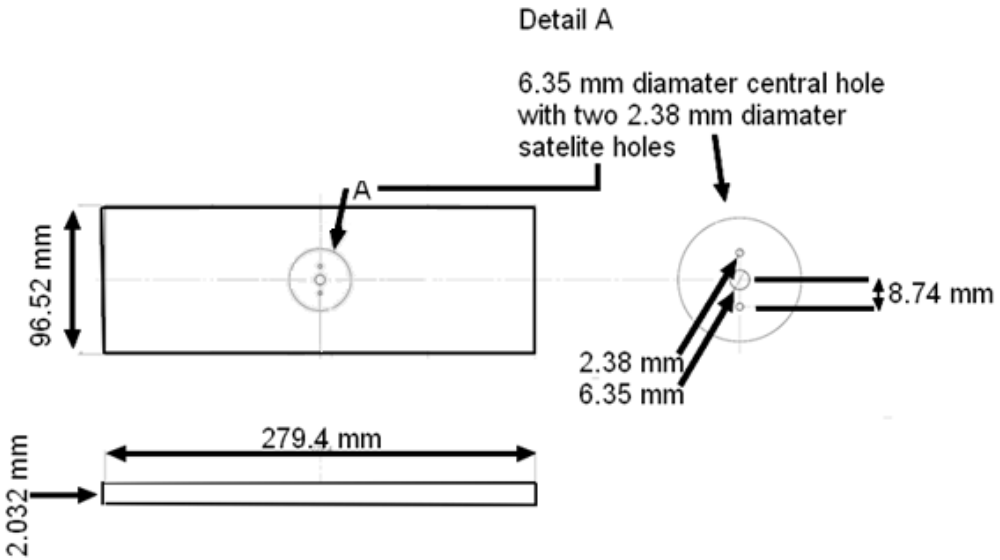

Figure 1. Schematic of the DNH coupon, from [38].

In this study attention was focused on specimens which had the fastest growing crack growth rates, viz: specimens P3-IG-33, P3-IG-16, P3-IG-04 and P3-IG-01. In specimens P3-IG-33, P3-IG-16 the IGC was approximately 1.5 mm and 0.8 deep respectively. These specimens were subjected to a measured RAAF FCA-352 (clipped) flight load spectra. Specimens P3-IG-04 and P3-IG-01, where the IGC was approximately 0.42 mm and 0.33 deep respectively, were tested under a RAAF FCA-16 (clipped) flight spectrum, see [38] for more details. Both the spectra and the crack growth data are discussed in [38].

Preprints (www.preprints.org) | NOT PEER-REVIEWED | Posted: 12 June 2018 doi:10.20944/preprints201806.0174.v1

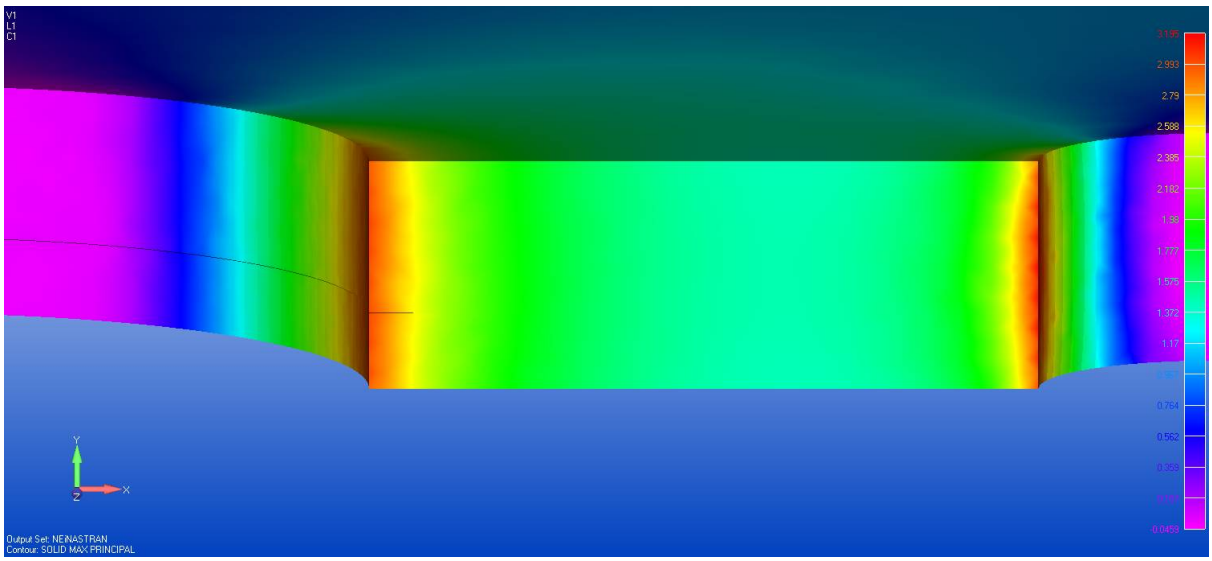

Figure 2. FEA model of dome nut hole coupon with an 0.8 mm deep IGC representing the IGC found in test specimen P3-IG-16, [38].

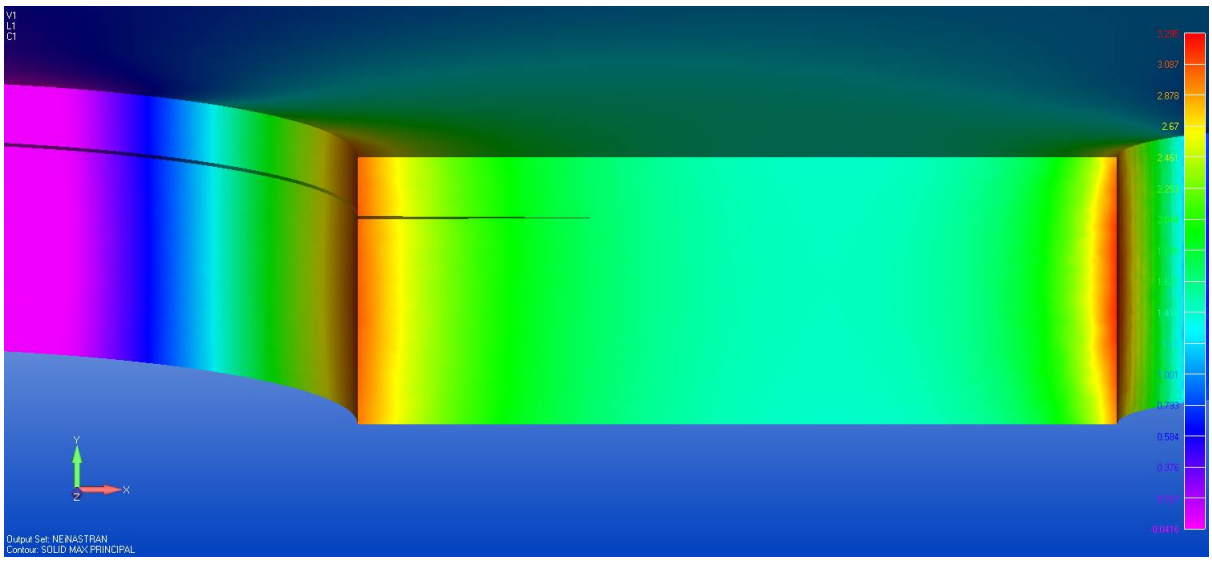

Figure 3. FEA model of dome nut hole coupon with an 1.5 mm deep IGC representing the IGC found in test specimen P3-IG-33, from [38].

 doi:10.20944/preprints201806.0174.v1

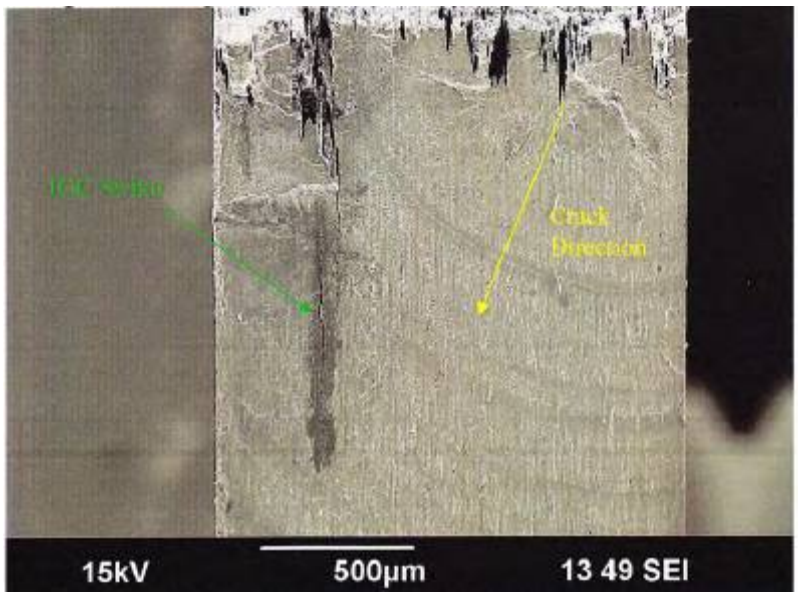

Figure 4. Local view of the fracture surface corresponding to test specimen P3-IG-33, from [38].

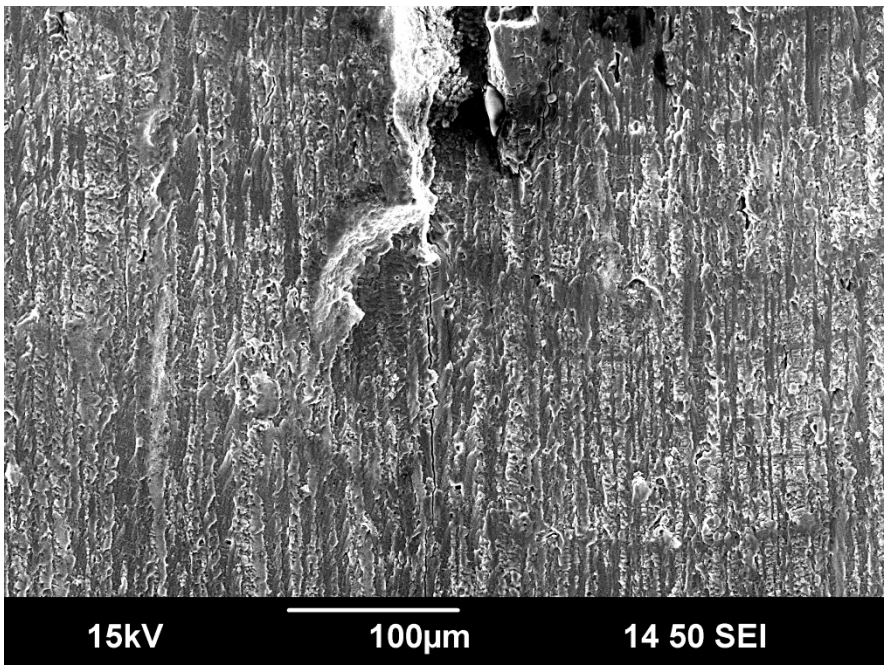

Figure 5. Local view of the fracture surface corresponding to test specimen P3-IG-16, from [38].

2.1. Crack growth in DNHS specimens tested under a measured RAAF AP-3C flight load spectrum

In [38] three dimensional finite element models were created for each specimen. Models were created for specimens both with and the without IGC. In each case crack growth was allowed to develop naturally and the associated stress intensity factors were computed using three dimensional weight function theory as explained in [19, 34]. The advantage of this formulation is that cracks do not have to be explicitly modelled, there is no restriction on the aspect ratio's, which are allowed to change as the crack(s) grow, and only the uncracked finite element model is required, see [19] for more details. In this instance [38] revealed that for specimen P3-IG-33 the IGC was located close to what we will term the "upper surface" of the specimen, see Figures 2 and 3 where the IGC is approximately 0.3 mm beneath the surface. Reference [38] also revealed that for this specimen the initiating feature appeared to lie near the upper intersection of the surface of the "lower" IGC and the bore of the hole, i.e. in the larger

Preprints (www.preprints.org) | NOT PEER-REVIEWED | Posted: 12 June 2018 doi:10.20944/preprints201806.0174.v1

ligament. The precise location of the IGC is given in [38]. To evaluate the effect of different initial crack configurations analysis on crack growth in specimens P3-IG-04 and P3-IG-01 two types of initial crack configurations were analysed, viz: an initial corner crack and an initial semi-elliptical crack that spans the IGC, as was the case when there was no IGC. In each case, as in all of the analyses performed in this report, the depth of the initial equivalent precrack (EPS) was taken as per [17, 40] to be 0.01 mm.

As recommended in [8, 19] the computed crack growth histories were obtained using the Nasgro crack growth equation for this material, viz:

$$da/dN = 1.86\ 10\text{-}9\ [(\Delta K - \Delta K_{thr})^2/(1\text{-}Kmax/111) \qquad (2)$$

with the constants for this material as given in [19]. The computed crack growth histories are shown in Figure 6 together with the measured crack length histories. Here the term ΔK_{thr} accounts for the fatigue threshold, see [8, 19] for more details. As can be seen in Figure 6 the computed and measured crack growth histories are in good agreement. Of particular interest is the fact that, in this instance, the computed results with and without IGC were almost identical. This reflects the fact that IGC does not significantly change the local stress field.

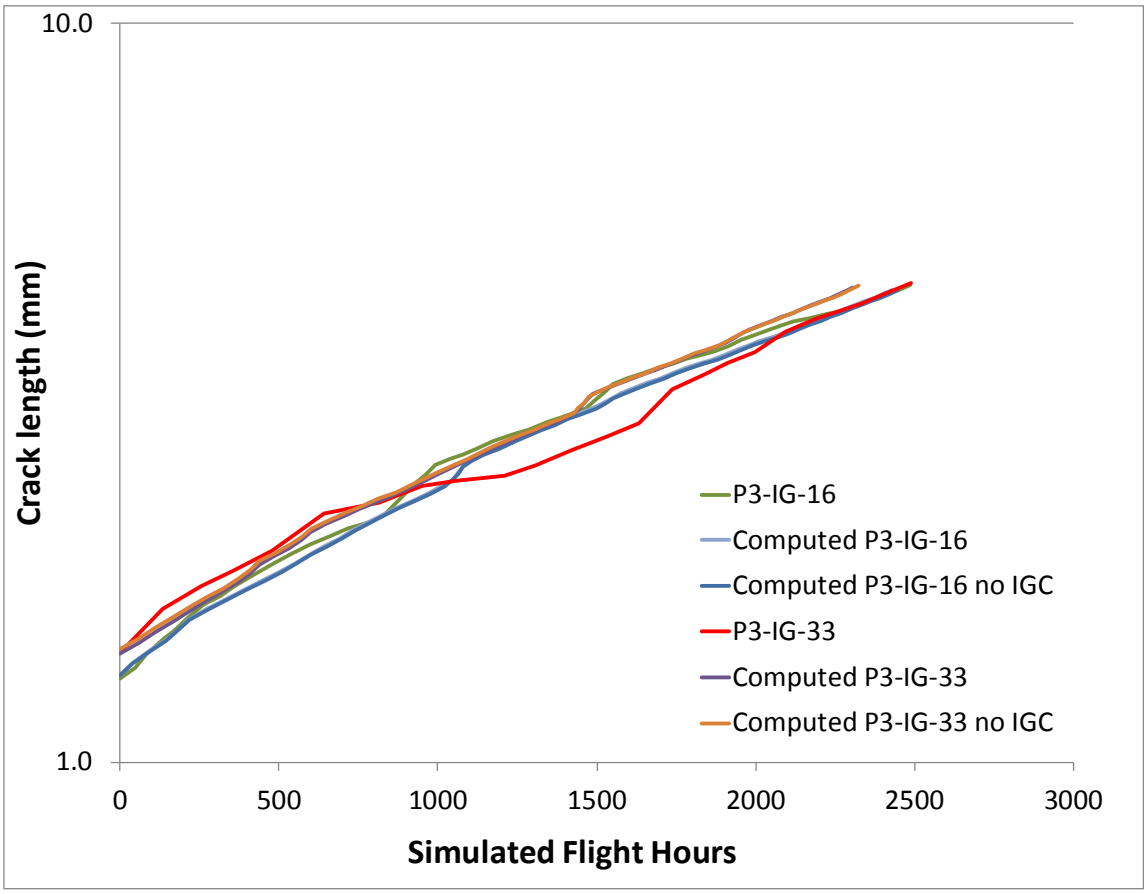

Figure 6. Comparison of the computed and measured crack growth histories for specimens P3-IG-16 and P3-IG-33, from [38].

References [7, 8, 19, 26, 27, 38] illustrated how the variation in the crack growth histories can be reasonably well captured by allowing for small changes in the threshold term ΔK_{thr}. The variation in the measured and computed crack growth histories for test specimens P3-IG-03, P3-IG-16, P3-IG-24 and P3-IG-032 is shown in Figure 7 along with the computed crack growth histories where the associated values of the threshold ΔK_{thr} used in the analysis are given in Table 1. Here it is clear that both the crack growth history associated with the fastest growing cracks and the scatter in the measured crack growth histories are captured quite well. It is also clear that:

Preprints (www.preprints.org) | NOT PEER-REVIEWED | Posted: 12 June 2018 doi:10.20944/preprints201806.0174.v1

i) The fastest cracks, i.e. the lead cracks, grow exponentially as per the USAF approach to risk assessment [16] and the DST Group formulation [17, 18] that was originally developed for assessing the structural integrity of the RAAF F/A-18 Classic Hornet fleet [18].

ii) For such naturally occurring lead cracks the fatigue threshold term ΔK_{thr} is quite small, see Table 1.

iii) The presence of IGC made little difference on the computed crack growth history.

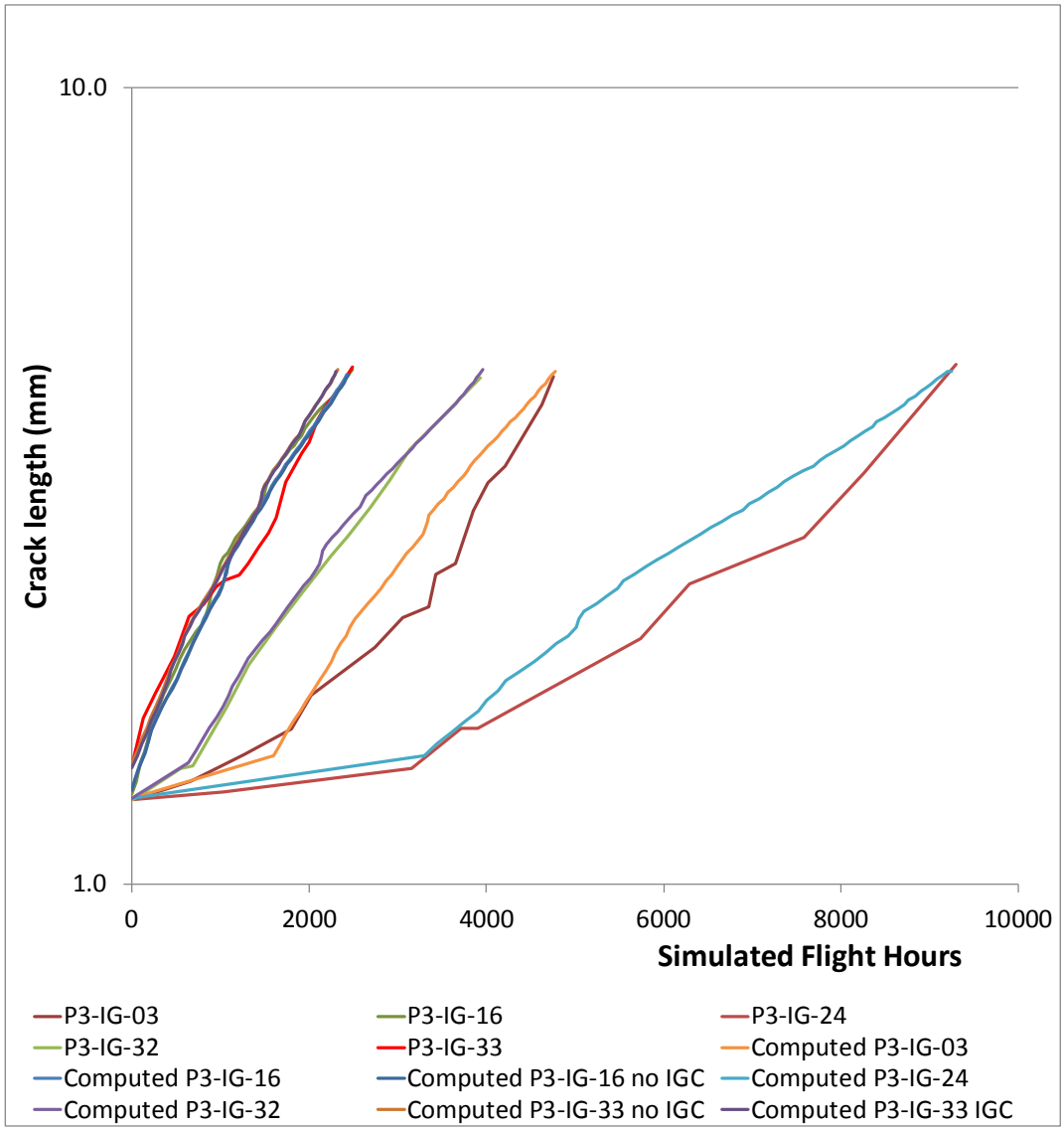

Figure 7. Comparison of the computed and measured crack growth histories for specimens P3-IG-16 and P3-IG-33, from [38].

Table 1. Values of the threshold used, from [38].

Test Specimen	ΔK_{thr} (MPa $\sqrt{m}$)
P3-IG-03	1.2
P3-IG-16	0.2
P3-IG-24	1.6
P3-IG-32	0.6
P3-IG-33	0.2

Preprints (www.preprints.org) | NOT PEER-REVIEWED | Posted: 12 June 2018 doi:10.20944/preprints201806.0174.v1

3. Crack Growth at Fastener Holes Containing Intergranular Cracking

Having established how the Hartman-Schijve crack growth equation can be used to accurately compute the growth of cracks at a fastener hole containing intergranular cracking subjected to a measured operational maritime flight load spectrum let us next consider the problem discussed in [20] which involves the growth of cracks from surface pits under a representative civil aircraft spectrum. (Here it should be noted that the ability of this formulation to accurately compute the growth of cracks from surface pits under combat aircraft flight load spectra is shown in [8, 19, 20, 26, 41] and its ability to accurately compute the growth of cracks from surface corrosion in a bridge steel is illustrated in [42].) The test coupons discussed in [20] were made from an AA7050-T7451 6" thick plate and had an "hourglass" (dogbone) shape, as shown schematically in Figure 8. The mechanical properties of the plate are detailed in Table 2.

The specimens were designed to have geometric features similar to the critical Outer Mould Line (OML) flange area just below one of the lower wing attachment lugs of the F/A-18 aircraft. The surface of the coupon was etched using a treatment similar to that used by Boeing to etch components of the F/A-18 prior to coating with Ion Vapour Deposited (IVD) aluminium. As explained in [20] the pitting produced by the etching process produces pits of the order of 10μm deep and as such are also of a size typical of other discontinuities in this material i.e. inclusions and small pores [17]

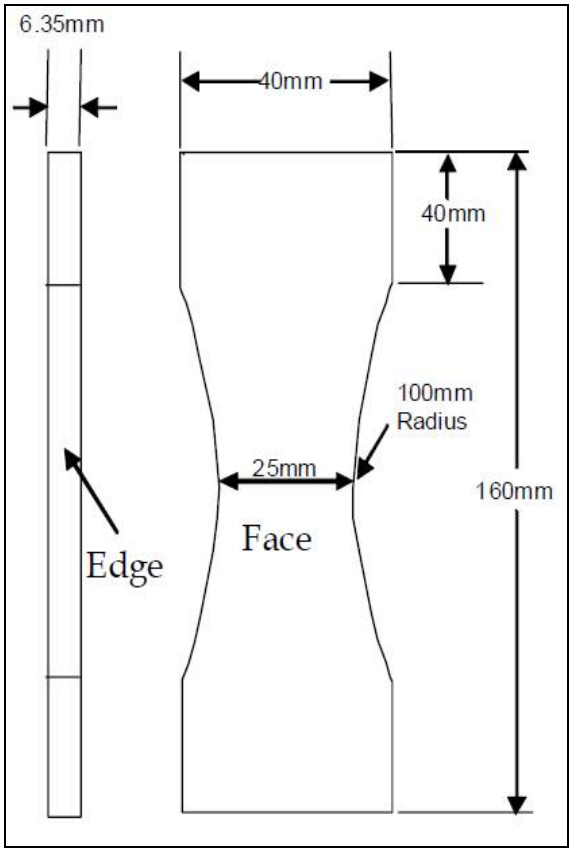

Figure 8. Geometry of the test specimens, from [20].

 doi:10.20944/preprints201806.0174.v1

Table 2. Mechanical properties of the 7050-T7451 plate, from [20].

Property	LM plate
Thickness	6.35mm (1/4 inch)
Test Section Width	25mm
Radius	47.1mm
Total Width	25mm
Total Length	160mm
Cross-sectional Test Area (At)	158.75mm^2
Stress Concentration Factor	1.155
Load Direction	[L]
Surface Finish	Simulated pre-IVD
Plate UTS (L. LT, ST)	483.3, 488.8, 472.3 MPa

In [20] five coupons were fatigued at 10Hz under a miniTWIST spectrum, the load level used as given in Table 3, where one load block consisted on 62,892 cycles, see [20] for more details. The fatigue lives of these specimens are given in Table 4. Plots of the associated crack depth versus fatigue life histories are shown in Figure 9.

Table 3. Values of the threshold used, from [38].

Coupon	P_{max} (kN)	P_{min} (kN)	Net section peak applied stress (MPa)
LM296	47.748	-11.015	301
LM322	48.034	-11.307	303
LM340	47.887	-11.057	302
LM349	47.802	-11.032	301
LM354	47.901	-13.341	302

Table 4. Fatigue lives of the specimens, from [20].

Coupon	Life (Blocks)	Life (Cycles)
LM296	15.62	982085
LM322	11.66	733411
LM340	15.84	996092
LM349	17.00	1069179
LM354	16.39	1030801

The crack growth histories computed in [20] used the Hartman-Schijve equation for this material, viz:

$$da/dN=7\times 10^{(-10)}\ (\Delta K-\Delta K_{thr}/\sqrt{(1-K_{max}/47)})^2 \qquad (3)$$

and are also shown in Figure 9. Here it can again be seen that the growth of both long and short cracks growing from etch pits on the surface of an AA7050-T7451 coupon, which was cycled under the miniTWIST spectrum, can be reasonably accurately captured by allowing for relatively small

Preprints (www.preprints.org) | NOT PEER-REVIEWED | Posted: 12 June 2018 doi:10.20944/preprints201806.0174.v1

changes in the ΔKthr value. The values of ΔK_{thr} used as well as the initiating discontinuity size are shown in Table 5.

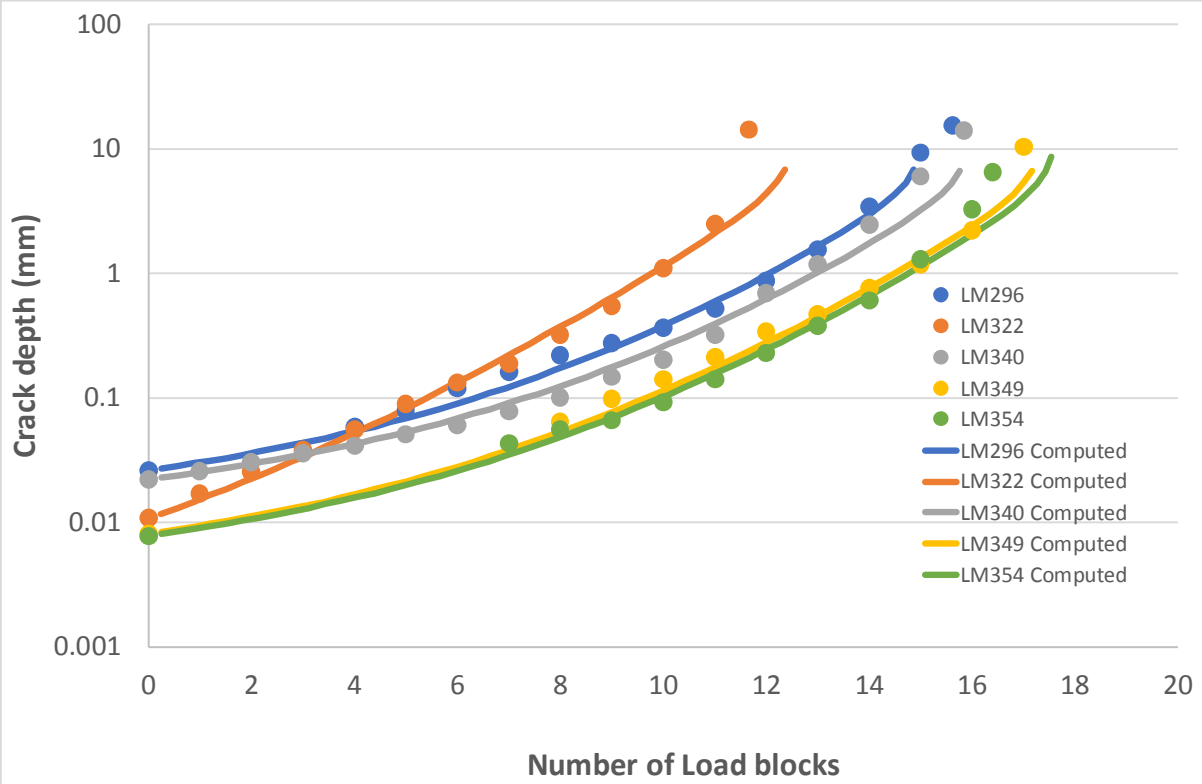

Figure 9. Comparison of measured and computed crack growth histories of AA7050-T8451 under a miniTWIST spectrum, from [20].

Table 5. Fatigue lives of the specimens, from [20].

Coupon	Life (Blocks)	Life (Cycles)
LM296	15.62	982085
LM322	11.66	733411
LM340	15.84	996092
LM349	17.00	1069179
LM354	16.39	1030801

The results of this study when taken in conjunction with that in Section 2 and the studies presented in [6, 8, 19, 20, 26, 4238, 41, 42] illustrate how the growth of cracks from environmental damage in aircraft structures can be reasonably accurately computed using the Hartman-Schijve crack growth equation and that allowing for experimental error the variability of the crack depth histories can be reasonably well accounted for by allowing for small changes in the value of the term Kthr. We also see that, as per the USAF approach to risk assessment [16] and the DST Group formulation [17, 18] the growth of the lead cracks, i.e. the fastest growing cracks, is approximately exponential. This observation, i.e. exponential crack growth, also holds for composite and cold spray repairs to cracks and for cold spray repairs to cracks that grow from holes that contain intergranular cracking [43, 44].

Preprints (www.preprints.org) | NOT PEER-REVIEWED | Posted: 12 June 2018 doi:10.20944/preprints201806.0174.v1

4. INTERPRETING THE EFFECT OF THE ENVIRONMENT ON da/dN VERSUS ΔK CURVES

The paper by Jones, Peng, Singh, Huang and Tamboli [6] revealed that the accelerated crack growth rate seen in tests in laboratory tests in an aggressive environment can often be accounted for by allowing for the effect of the environment on the fatigue threshold term ΔK_{thr}. However, since as we have seen in the preceding sections lead cracks in operational aircraft generally have a low threshold this effect, although significant in laboratory tests performed in accordance with the main body of the test standard ASTM E647-13a, will often be minimal for cracking in operational aircraft. As a result laboratory tests on small sub mm cracks tested in an aggressive environment often yield da/dN versus ΔK curves that essentially coincide with the small crack curves associated with laboratory tests in room temperature environments [6, 8].

To illustrate that the effect of the environment can sometimes be represented by allowing for its effect on the value of ΔK_{thr} consider the data presented by Wanhill [45] for the crack growth in the commercial titanium alloy IMI130 tested in dry argon (less than 20 ppm water vapour), normal air (40-60% relative humidity) and 3.5% aqueous NaCl. The associated da/dN versus ΔK curves are given in Figure 10. Figure 11 presents this data replotted as per equation (1), i.e. by plotting da/dN against $(\Delta K-\Delta K_{thr})/\sqrt{(1-K_{max}/A)}$. Here we see that the various curves now (essentially) all fall onto a single curve regardless of the R ratio or the test environment, i.e. that the difference in the crack growth rates can be accounted for by allowing for changes in the term ΔK_{thr}. The values of ΔK_{thr} and A used in Figure 11 are given in Table 6.

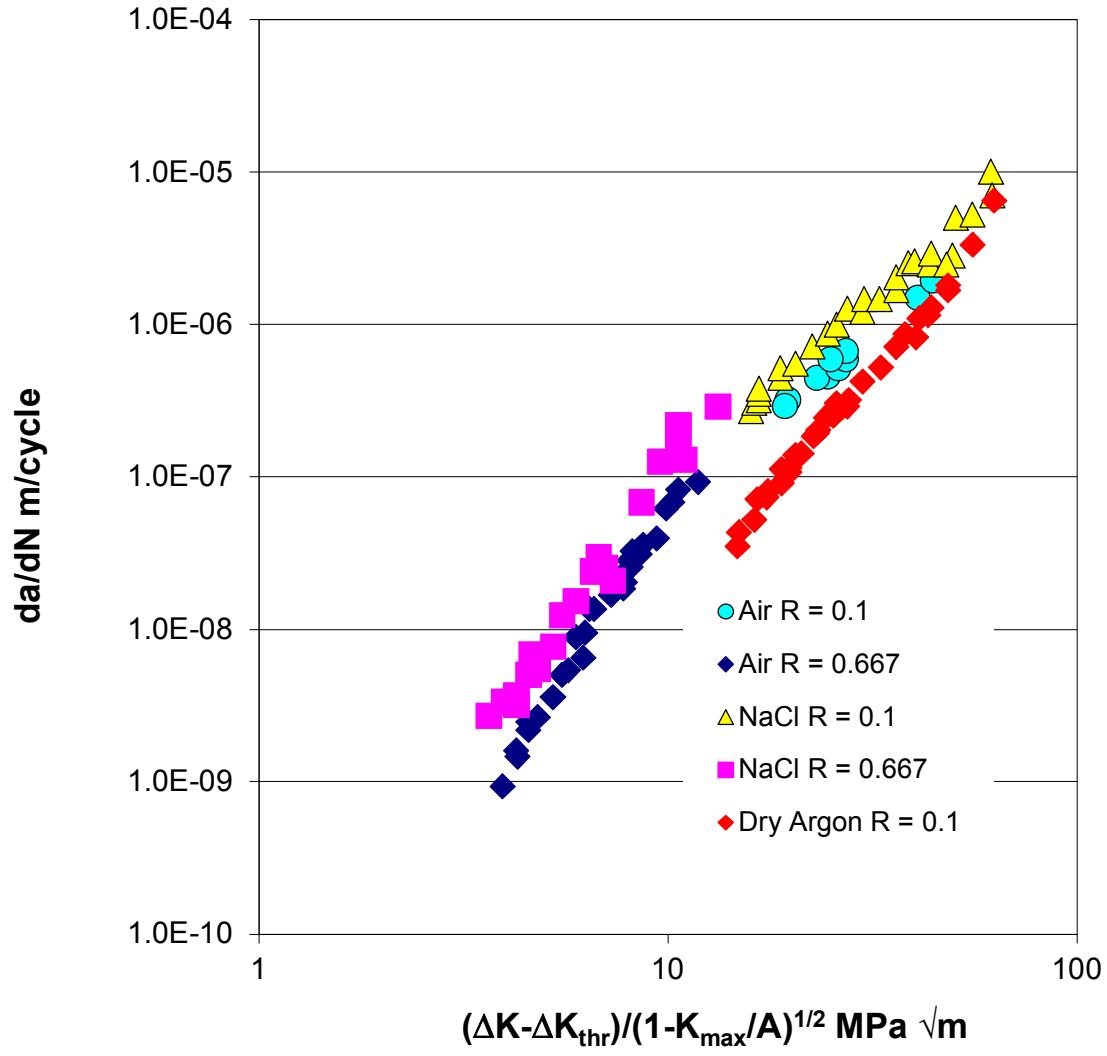

Figure 10. Crack growth in IMI130, from [45].

Preprints (www.preprints.org) | NOT PEER-REVIEWED | Posted: 12 June 2018 doi:10.20944/preprints201806.0174.v1

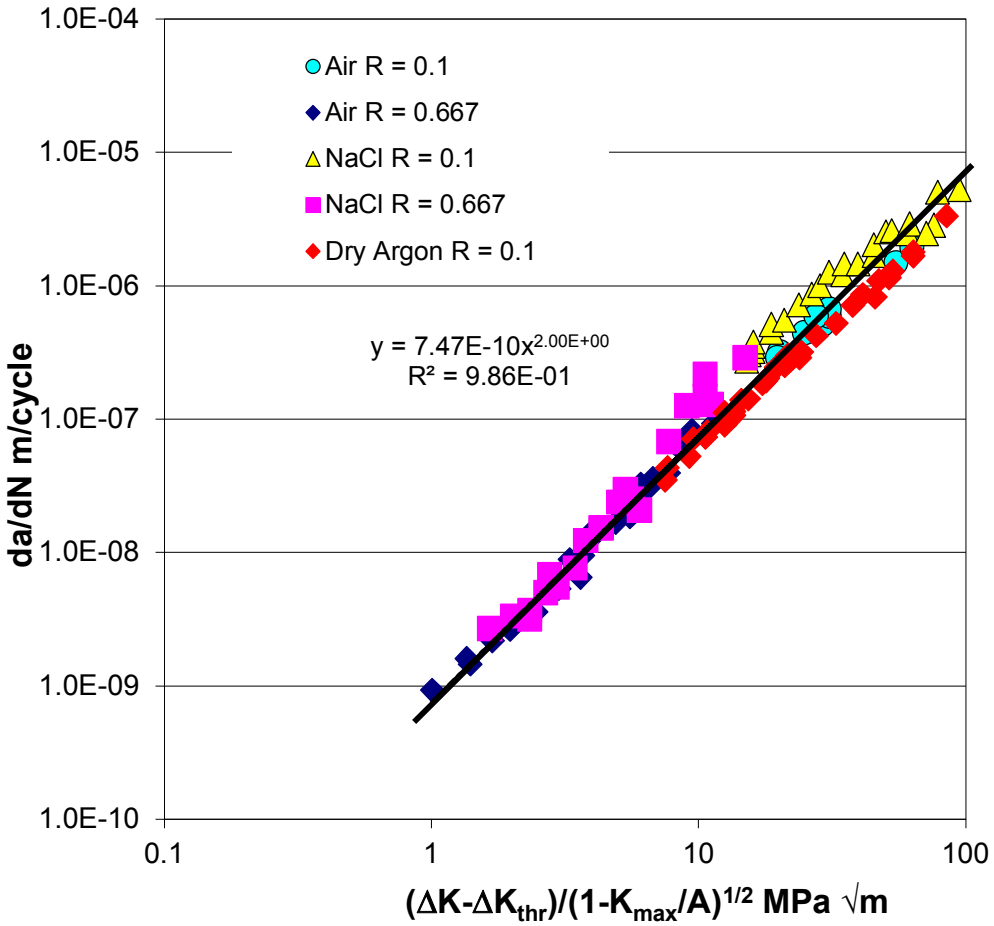

Figure 11. Crack growth in IMI130 replotted.

Table 6 Values of K_{thr} and A

Material	Environment	Nature of the test	Test frequency (Hz)	ΔK_{thr} (MPa √m)	A (MPa√m)
IMI130	Lab air	R = 0.1	30-50	2.4	90
IMI130	3.5% NaCl	R = 0.1	30-50	2.1	90
IMI130	Dry argon	R = 0.1	30-50	8.0	90
IMI130	Lab air	R = 0.667	30-50	3.0	90
IMI130	3.5% NaCl	R = 0.667	30-50	2.1	90
7075-T6511 (CT)	water vapour saturated with N_2	K_{max} = 15 (MPa √m)	10	1.1	30
7075-T6511 (SENT)	water vapour saturated with N_2	K_{max} = 15 (MPa √m)	10	2.0	30
7075-T6511 (small crack)	1% NaCl	K_{max} = 15 (MPa √m)	10	0.87	30
7075-T6511 (small crack)	Simulated lapjoint (SLJ) environment	K_{max} = 15 (MPa √m)	10	0.75	30
7055-T6511 (CT)	water vapour saturated with N_2	K_{max} = 15 (MPa √m)	10	0.8	30

Preprints (www.preprints.org) | NOT PEER-REVIEWED | Posted: 12 June 2018 doi:10.20944/preprints201806.0174.v1

7055-T6511 (SENT)	water vapour saturated with N_2	K_{max} = 15 (MPa √m)	10	1.8	30

4.1. *Anomalous crack growth curves*

There are times when environmental tests can yield apparently anomalous results. For example Kim, Burns and Gangloff [46] presented crack growth data for 7075-T6511 and 7055-T6511 tested in water vapour saturated with N_2 using both SENT and CT specimens, tested at a constant K_{max} = 17 MPa √m, and compared this data with that associated with the growth of (short) sub mm initial cracks, in aggressive environments ,with depths that varied between 0.48 to 0.84 mm. This data revealed that the SENT and CT specimens, which are both ASTM E647-13a standard test specimen geometries, gave very different da/dN versus ΔK data, see Figure 12. However, as shown in [47] the anomaly vanishes when the data is replotted as per equation (1), i.e. when plotting da/dN against $(\Delta K-\Delta K_{thr})/\sqrt{(1-K_{max}/A)}$, see Figure 13. Figure 13 also reveals that, for the growth of small cracks in 7055-T651, when expressed as per equation (1) the long and small crack data now essentially fall onto the same curve, i.e. that in this instance the small crack anomaly vanishes when allowance is made for the reduction in ΔK_{thr}. Furthermore, the various tests can all be approximated by the relationship

$$da/dN = 1.86\ 10^{-9}\ [(\Delta K - \Delta K_{thr})^2/(1-K_{max}/A)] \quad (3)$$

that was determined in [41] for the growth of long cracks in 7075-T6511 in room temperature laboratory conditions. The values of ΔK_{thr} and A used in Figure 13 are given in Table 6.

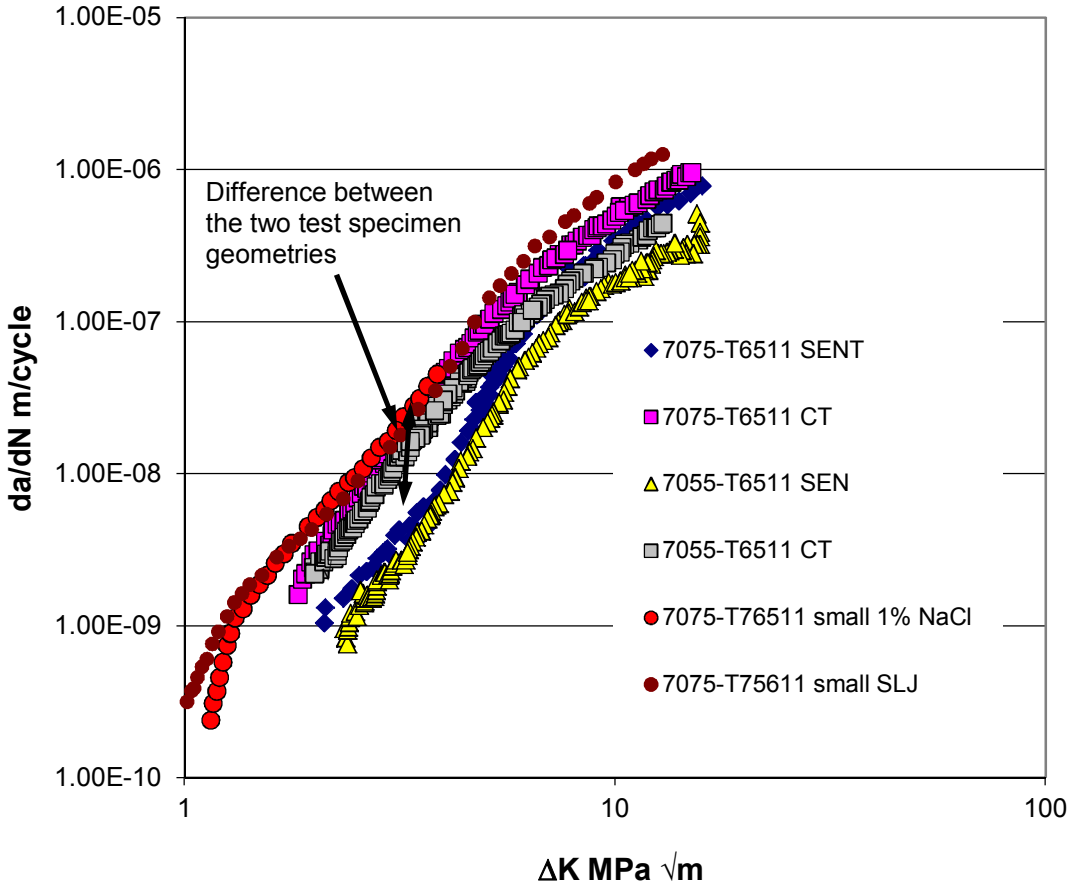

Figure 12. Crack growth in 7075-T651 and 7055-T6511 tests, from [46]. (SLJ = simulated lap joint environment).

Preprints (www.preprints.org) | NOT PEER-REVIEWED | Posted: 12 June 2018 doi:10.20944/preprints201806.0174.v1

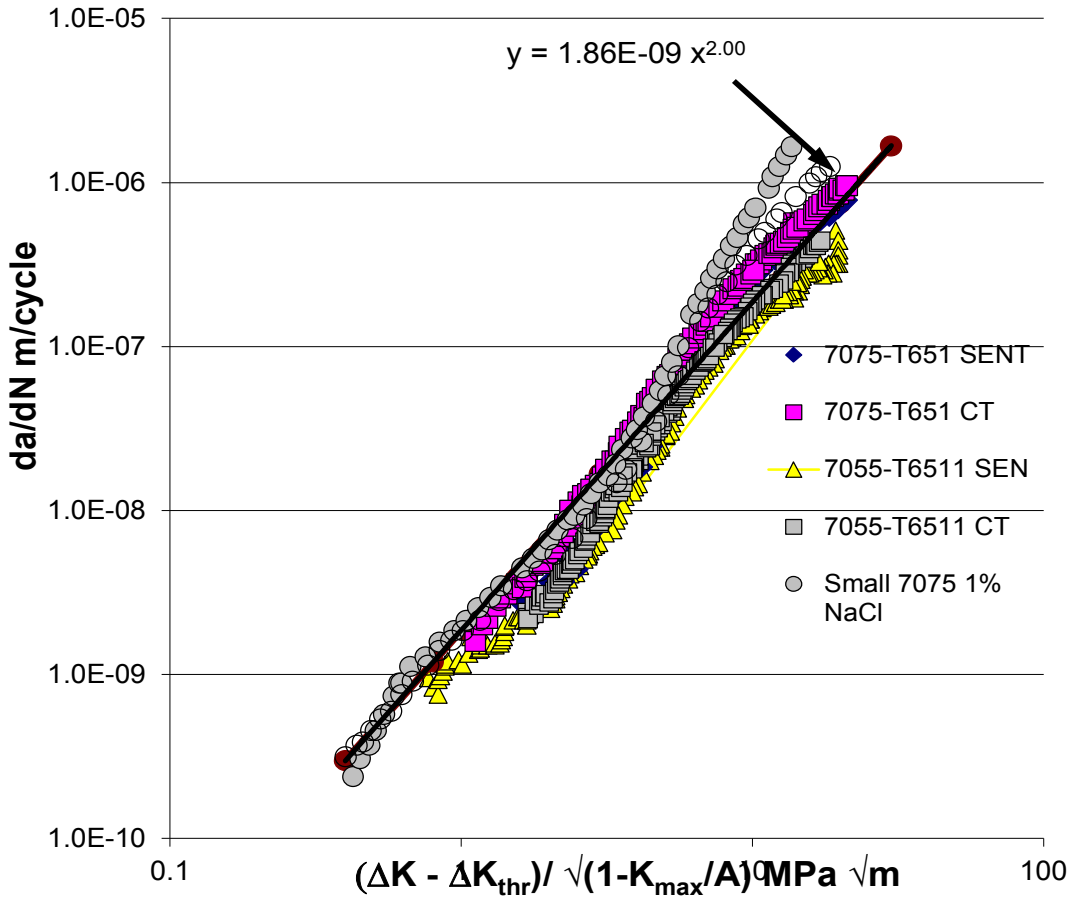

Figure 13. Crack growth in 7075-T651 and 7055-T6511 tests replotted, from [47].

As such we see that when assessing the effect of the environment on tests performed as per the main body of the test standard ASTM E647-13a it is desirable to check to see if the phenomena observed can be captured by merely allowing for changes in the threshold term ΔK_{thr} or if there are marked changes in the values of D and β in equation (1).

5. STRESS CORROSION CRACKING (SCC)

Having initially focused on the growth of cracks from environmentally induced cracking let us next address the problem of stress corrosion cracking (SCC) in rib stiffened wing planks. This problem is common to both military transport and maritime reconnaissance aircraft. Stress corrosion cracks arising in the wing planks of C-130 Hercules and P3C Orion aircraft are a good examples of this problem, see Figures 14 and 15. In both instances the wing planks were machined from monolithic 7075-T6 rolled plate material to produce wing skins with integral reinforcing risers, about 2.6 mm thick.

Preprints (www.preprints.org) | NOT PEER-REVIEWED | Posted: 12 June 2018 doi:10.20944/preprints201806.0174.v1

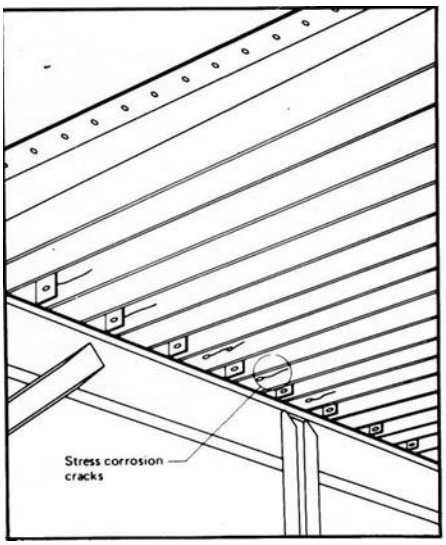

Figure 14. Schematic diagram of location of stress corrosion cracking in C-130 wing, from [48].

Figure 15. Typical SCC in a P3C (Orion) wing, photograph courtesy of M. Dorman, RAAF MPSO.

On compression surface of the wing the allowable size of the SCC is generally set by the length that will cause local buckling of the wing [44, 49]. To illustrate effect of SCC on the load carrying capacity [49] tested three nominally identical specimens. The geometry of the test specimens are shown in Figures 16 and 17. This included two baseline specimens, i.e. no simulated SCC, and one specimen with simulated SCC. All of the specimens were cut from a RAAF AP3C (Orion) wing panel supplied by Maritime Systems Patrol Office and Airbus Group Australia Pacific, see Figure 18. As such although the specimens were nominally identical the specimens had small differences in the thicknesses of the riser (stiffeners), see Table 7.

Table 7 Difference in thicknesses of the riser, from [49].

Specimen Identifier	Thickness (mm)
1 (no SCC)	4.22
2 (no SCC)	4.20
3 (SCC)	4.29

Preprints (www.preprints.org) | NOT PEER-REVIEWED | Posted: 12 June 2018 doi:10.20944/preprints201806.0174.v1

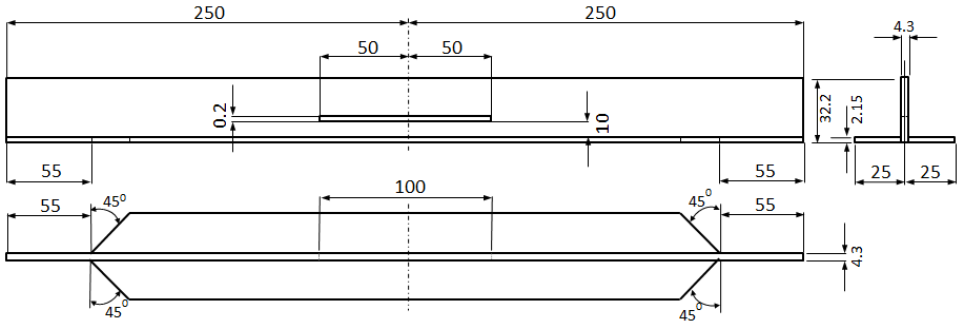

Figure 16 - Geometry of the test specimen with simulated SCC, from [**Error! Reference source not found.**49].

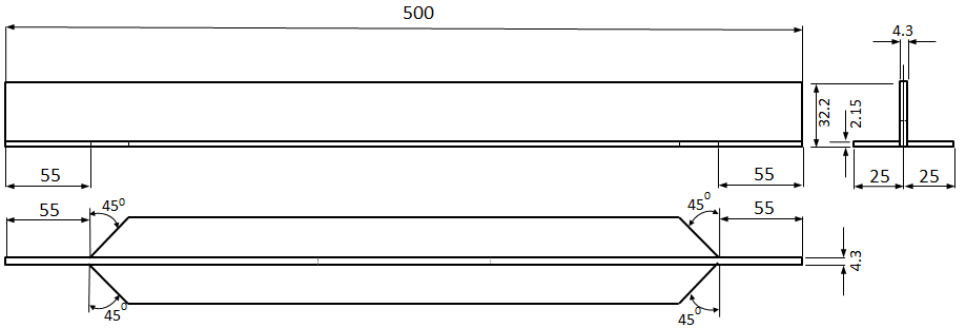

Figure 17 - Geometry of the baseline specimen (no simulated crack), from [**Error! Reference source not found.**49].

Figure 18 - Exterior (a) and interior (b) views of a right hand wing upper wing panel (part number 938807-102), from [**Error! Reference source not found.**].

The buckled shapes for three types of specimens are shown in Figure 19 and the associated load deflection curves are shown in Figure 20. Here we see that not only did SCC dramatically lower the failure load it also significantly changed the failure mode from a "global" buckling failure to local failure which resulted in cracking that ran the entire length of the specimen.

The buckled shapes for three types of specimens are shown in Figure 19 and the associated load deflection curves are shown in Figure 20. Here we see that not only did SCC dramatically lower the failure load it also significantly changed the failure mode from a "global" buckling failure to local failure which resulted in a cracking that ran the entire length of the specimen.

Preprints (www.preprints.org) | NOT PEER-REVIEWED | Posted: 12 June 2018 doi:10.20944/preprints201806.0174.v1

(a)

(b)

Figure 19 - The buckled shapes, (a) with simulated SCC, (b) baseline specimen, from [**Error! Reference source not found.**].

The difference in the load deflection curves arising due to the presence of SCC is shown in Figure 20. Here, in addition to the dramatic reduction in strength due to the SCC, we see that prior to failure the compliance of the specimen was unchanged by the presence of SCC. This suggests that the presence of SCC will not affect the load flow in a wing plank and hence not compromise the structural integrity of any nearby structural repairs.

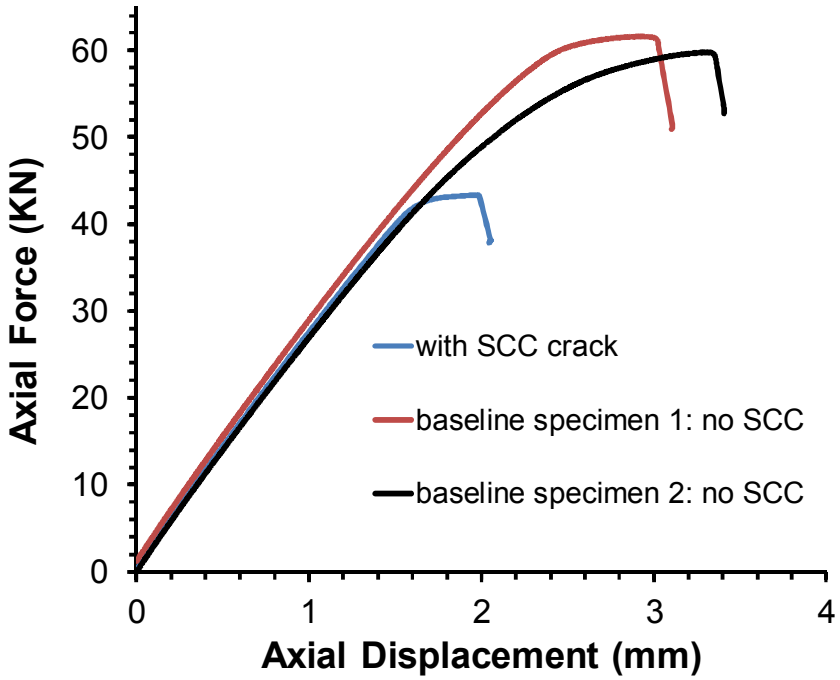

Figure 20 - Load displacement curves, from [**Error! Reference source not found.**49].

Preprints (www.preprints.org) | NOT PEER-REVIEWED | Posted: 12 June 2018 doi:10.20944/preprints201806.0174.v1

A finite element study into the effect of SCC on the buckling modes and buckling loads was also performed in [49]. This study revealed that the computed and experimental buckling loads were in good agreement, see Table 8, thus confirming the ability of finite element analysis to be used to assess the effect of SCC on a structure.

Table 8 Comparison between the experimental and FEM buckling loads, from [**Error! Reference source not found.**].

Specimen No.	Experimental (kN) [Remote mean stress in MPa]	FEM (kN)	% difference
1 (no SCC)	60.2 [252]	60	-0.03
2 (no SCC)	59.8 [250]	60	0.3
3 (SCC)	41.3 [173]	42.8	0.35

6. ASSESSMENT OF THE EFFECT OF SKIN CORROSION ON WING PLANK INTEGRITY ON COMPRESSIVE SURFACES

Having briefly introduced the problem of corrosion on upper wing skins this section focuses on a typical AP3C wing plank with skin corrosion that lies between two risers (stiffeners), see Figure 21. As outlined in [44], observed corrosion is often near circular in shape. However, because of the difficulty in analysing this geometry a full width corrosion grindout is often assumed when the assessment of the impact of corrosion is conducted, see Figure 21. Consequently, to more closely represent the actual corrosion profiles [44] studied the effect of circular corrosion that lay between two risers. In [44] special attention was paid to the US Joint Services Structural Guidelines JSSG2206 requirement that there must be no yielding at 115% Design Limit Load (DLL). As such one of the primary assessment criteria used in [44] was that the corrosion did not violate the DDL requirements in JSSG2006 that there should be no local yielding at 115% DLL.

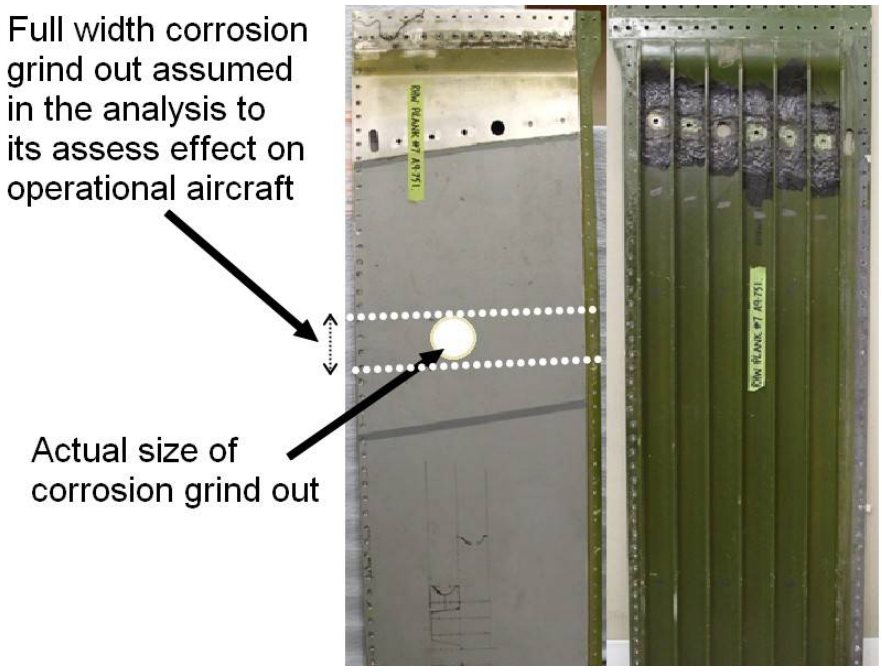

Figure 21 - Exterior and Interior Views of RHW#07 Upper Wing Panel (P/N 938807-102), from [44].

6.1. *Corrosion between risers*

The geometry of the panel and risers analysed in [44] was taken so as to represent a typical AP3C wing section. To this end [44] analysed a 500 mm (long) by 250 mm (wide) rib stiffened 7075-T6 aluminium alloy panel where the skin and the risers were both 4.3 mm thick. The length of the panel was taken so as to approximate the distance been the H-clips that are attached to the risers, see Figures 22 and 23. The risers were 30 mm deep and 50 mm apart. The skin thickness analysed was 2.1 mm. In this study the corrosion was taken to be 40 mm in diameter with a depth of 1.05 mm. This depth of corrosion was approximately 50% of the total thickness of the skin. As such the panel would normally be replaced/rejected.

Figure 22 - Underside of a typical P3C wing plank showing the attachment points, from [44].

Figure 23 - Underside of a typical P3C wing plank showing the attachment points, from [44].

6.2. *Assessment of corrosion*

The finite element model developed in [44] consisted of 961,579 nodes and 583,696 twenty one node isoparametric element elements. Both a liner buckling analysis and a non-linear analysis, allowing for both material (material yielding) and geometric nonlinearities (large displacements), were performed. This analysis used the stress strain curve for the material as given in Mil Handbook 5. A linear buckling analysis of the baseline (no corrosion) panel was conducted first. This yielded a buckling load of 325 kN. The associated buckling mode is shown in Figure 24. The linear buckling

Preprints (www.preprints.org) | NOT PEER-REVIEWED | Posted: 12 June 2018 doi:10.20944/preprints201806.0174.v1

load for a 50% loss of skin was found to be 318 kN. The associated buckling mode is shown in Figure 25. At first glance these results would appear to suggest that corrosion has little effect on the failure load. However, as shown in [44] this conclusion is incorrect.

Figure 24 - Buckling loads for the baseline panels (no corrosion), from [44].

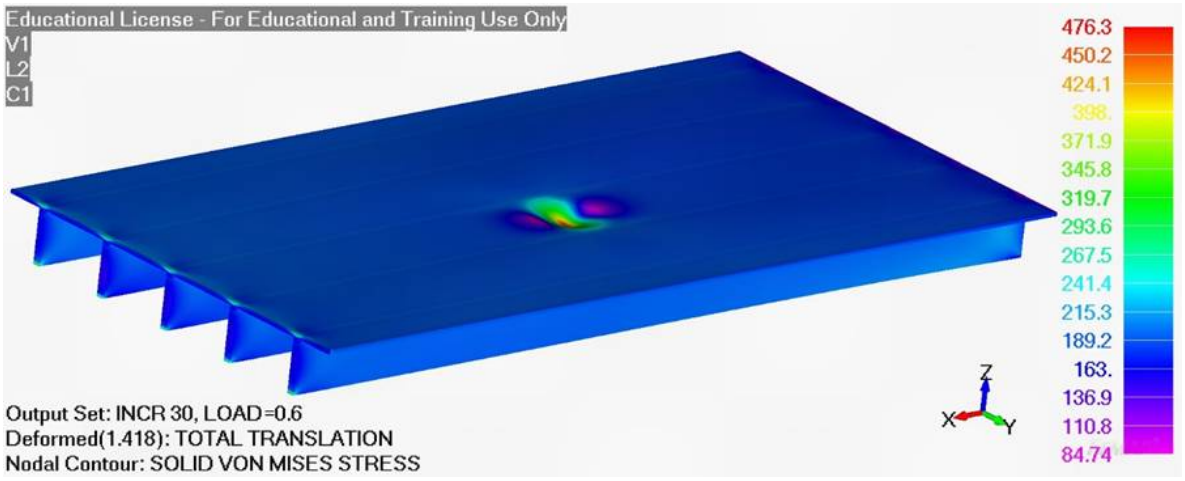

Figure 25 - Buckling mode and buckling load (318 kN), from [44].

To further evaluate this conclusion a non-linear analysis, allowing for both material (material yielding) and geometric nonlinearities (large displacements), was performed. This analysis revealed that, for the case of a 50% loss of material, the load to first yield, and hence the maximum load carrying capacity allowed if the design guidelines as delineated in JSSG2006 are to be met, was approximately 240 kN which is significantly below the linear buckling load of approximately 318 kN. Figure 26 present the stress field at the onset of yielding, i.e. at a load of approximately 240 kN and an average panel stress of approximately 205 MPa.

At this point it should also be noted that the presence of skin corrosion has changed the failure mode from global failure (overall panel buckling) to a local failure mode, which is relatively unaffected by the nature of the constraints applied to the non-loaded edges, whereby the remaining material fails by exceeding material allowables.

Preprints (www.preprints.org) | NOT PEER-REVIEWED | Posted: 12 June 2018 doi:10.20944/preprints201806.0174.v1

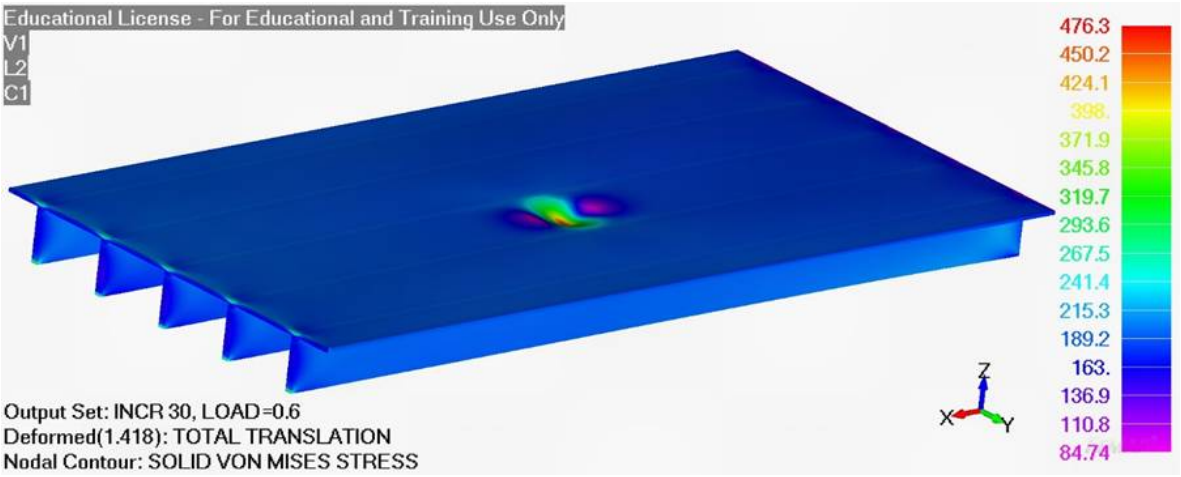

Figure 26 - Stress in the remaining material at a load of 240 kN, from [44].

7. DISCUSSION OF RESULTS

This paper has examined the combined effect of corrosion and fatigue on the growth of cracks in aircraft. It is shown that the growth of cracks from surface pitting and also from intergranular cracking at a fastener hole can be accurately computed using the Hartman-Schijve crack growth equation with the threshold term set to a small value. Furthermore both studies support the lead crack approach that has been independently developed by the USAF and the Australian Defence Science Technology Group that the growth of lead cracks in operational aircraft is often exponential.

It is also shown that what at first glance appears to anomalous crack growth data can be due to the effect of the environment on the fatigue threshold term ΔK_{thr} and that in the tests discussed the small crack anomaly could be accounted for by allowing for changes in the threshold term ΔK_{thr}.

It is further shown that finite element analysis can be used to compute the effect of environmentally induced skin corrosion and stress corrosion cracking in the ribs on the load bearing capacity of rib stiffened aircraft wings. In the case of skin corrosion it is shown that assessment of its effect on the load bearing capacity of the wing should involve an assessment of whether at 115% DLL the remaining material exceeds the yield stress of the material.

Author Contributions: Conceptualization, Rhys Jones, Neil Matthews and Nam Phan.; Methodology, Rhys Jones, Neil Matthews; Software, Daren Peng and Rhys Jones.; Validation, Rhys Jones and Daren Peng; Formal Analysis, Rhys Jones; Investigation, Rhys Jones and Daren Peng.; Resources, Neil Matthews and Nam Phan; Data Curation, Daren Peng; Writing-Original Draft Preparation, Rhys Jones; Writing-Review & Editing, Neil Matthews; Visualization, Daren Peng; Supervision, Neil Matthews; Project Administration, Neil Matthews.; Funding Acquisition, Nam Phan and Neil Matthews.

Funding: This research received no external funding.

Conflicts of Interest: The authors declare no conflict of interest.

Appendix: The Hartman-Schijve variant of the NASGRO crack growth equation

There are numerous crack growth equations that have been developed over the decades. The NASGRO equation developed by Forman and Mettu [50] is one of the most widely used equations and is available with both the NASGRO, AFGROW and FASTRAN computer codes. The Hartman-Schijve variant of the NASGRO equation, which is discussed in more detail in [8, 19], relates da/dN to the quantity by which ΔK exceeds a fatigue threshold ΔK_{thr} is given by:

$$da/dN = D((\Delta K - \Delta K_{thr})/\sqrt{((1-K\_max/A))})^{\beta} \quad (A1)$$

 doi:10.20944/preprints201806.0174.v1

Here D and β are constants, and A is the cyclic fracture toughness, a term which may differ from the fracture toughness K_c. ΔK_{thr} is defined as an apparent fatigue threshold and is dependent on crack length and R ratio. (Values of approximately 0.18 MPa $\sqrt{mm}$ were used in [7] to compute the growth of such lead cracks (also see [8, 19]) in 7050-T7451 and similar values were used for lead cracks in 7075-T6XX [19, 20, 26, 38].) The exponent β is often approximately 2 [8, 19]. Indeed, this finding is independently validated via the recent review of atomistic simulation of the growth of small cracks [52, 53]. As explained in ASTM E647-13a [54] and [8, 19, 20, 27-42, 53], for crack growth from small naturally occurring discontinuities there is little R ratio dependence and the value of ΔK_{thr} is very small . Hence there is little, if any, crack closure associated with the growth of small naturally occurring cracks [8, 19, 53].

Since the majority of the life of a fatigue crack is consumed in propagation of small cracks (up to about 1 mm), the understanding of small crack growth behaviour is crucial for fatigue life assessment, see ASTM E647-13a Appendix X3 [54] and [55]. It is now known [6-8, 15, 19, 20, 42, 38, 41, 27, 51, 53] that Equation (2) can capture the variation in the crack growth rates from small to long cracks by allowing for appropriate changes in the parameter ΔK_{thr}.

References

1. Wanhill R., Windisch M., Corrosion and Stress Corrosion Testing of Aerospace Vehicle Structural Alloys, SpringerBriefs in Applied Sciences and Technology, ISBN 978-3-319-89529-1.
2. Tiffany CF., Gallagher JP., Babish IV CA. (2010) Threats to aircraft structural safety, including a compendium of selected structural accidents/incidents, Aeronautical Systems Center, Engineering Directorate, Wright-Patterson Air Force Base, ASC- TR-2010-5002.
3. NTSB. (1989) Aircraft Accident Report, Aloha Airlines, Flight 243, Boeing 737-200, N73711, near Maui, Hawaii, April 28, 1988 (Aircraft Accident Report No. NTSB/AAR-89/03), Washington DC, National Transportation Safety Board.
4. FAA-2010-1280-001, Federal Register, Vol 76, 6, Monday January 2011, Rules and Regulations.
5. FAA AC No: 120-104, Establishing and implementing limit of validity to prevent widespread fatigue damage, 01/01/2011.
6. Jones R., Peng D., Singh RRK., Pu Huang, Tamboli D., Matthews N., (2015) On the growth of fatigue cracks from corrosion pits and manufacturing defects under variable amplitude loading, JOM, Vol. 67, No. 6, pp. 1385-1391.
7. Jones, R., Molent, L., Barter, S., Calculating crack growth from small discontinuities in 7050-T7451 under combat aircraft spectra, International Journal of Fatigue, 2013; vol. 55, pp. 178-182.
8. Jones R., Fatigue crack growth and damage tolerance, Fat Fract Eng Mat and Struct, 2014; 37, pp. 463-483.
9. Davis SL., DeGood K., Donohue N. and Goldberg D, (2013) The Fix We're In For: The State of Our Nation's Busiest Bridges, Transportation for America, http://t4america.org/docs/bridgereport2013/2013BridgeReport.pdf
10. http://www.railwayage.com/index.php/mechanical/freight-cars/ttci-rd-how-healthy-are-your-castings.html.
11. Final Report - Rail Inquiry 09-101 (incorporating 08-105): express freight train derailments owing to the failure of bogie side frames, various locations on the North Island Main Trunk, between 21 June 2008 and 7 May 2009 (www.taic.org.nz).
12. The Fix We're In For: The State of Our Nation's Busiest Bridges, Transportation For America//October 2011. Available on line at: http://t4america.org/docs/bridgereport/bridgereport-metros.pdf.
13. Connor RJ., Dexter R., Mahmoud H., Inspection and Management of Bridges with Fracture-Critical Details: A Synthesis of Highway Practice, National Cooperative Highway Research Program, NCHRP Synthesis 354, Transportation Research Board, Washington, D.C., 2005.
14. Mertz D., Steel Bridge Design Handbook: Design for Fatigue, U.S. Department of Transportation, Federal Highway Administration, Publication No. FHWA-IF-12-052 - Vol. 12, November 2012.
15. K. Ali, D. Peng, R. Jones, R. R. K. Singh, X. L. Zhao, A. J. McMillan, F. Berto, Crack growth in a naturally corroded bridge steel, Fatigue & Fracture of Engineering Materials & Structures, doi:10.1111/ffe.12568.
16. Berens AP., Hovey PW., Skinn DA., Risk analysis for aging aircraft fleets - Volume 1: Analysis, WL-TR-91-3066, Flight Dynamics Directorate, Wright Laboratory, Air Force Systems Command, Wright-Patterson Air Force Base, October 1991.
17. Barter SA., Molent L., Wanhill RH., The lead crack lifing framework, International Journal of Fatigue, 41, pp. 1-198, 2012.
18. Molent L., Jones R., (2016) A Stress versus Crack Growth Rate Investigation (aka Stress - Cubed Rule), International Journal of Fatigue, 87, pp, 435-443.
19. Jones R., Peng D., McMillan A., Crack growth from naturally occurring material discontinuities, Chapter 5, pp. 129-190, Aircraft Sustainment and Repair, Edited by R. Jones, N. Matthews, AA. Baker and V. Champagne Jr., Butterworth-Heinemann Press, 2018, ISBN 9780081005408.
20. Tamboli D., Barter S., Jones R., (2018) On the growth of cracks from etch pits and the scatter associated with them under a miniTWIST spectrum, International Journal of Fatigue, 109, pp. 10-16.
21. Molent, L. (2015). Managing airframe fatigue from corrosion pits - a proposal, Engineering Fracture Mechanics, Vol 137, pp 12-25.
22. Molent, L., Barter, S. and Wanhill, R.J.H. (2015). The decoupling of corrosion and fatigue for aircraft service life management, in Proceedings 28th ICAF Symposium, Helsinki, Finland.

23. Barter, S.A. and Molent, L. (2012). Investigation of an in-service crack subjected to aerodynamic buffet and manoeuvre loads and exposed to a corrosive environment in Proceedings of the 28th International Congress of the Aeronautical Sciences, Brisbane, Australia.
24. Barter SA. and Molent L., (2013) Service fatigue cracking in an aircraft bulkhead exposed to a corrosive environment, Engineering Failure Analysis, 34. 181-188.
25. Trathen, P. (2011). Corrosion monitoring systems on military aircraft in Proceedings of the 18th International Conference on Corrosion, Perth, Australia.
26. Burns, J.T., Gangloff, R.P. and Bush, R.W. (2011). Effect of environment on corrosion induced fatigue crack formation and early propagation in aluminium alloy 7075-T651 in Proceedings of DoD corrosion conference, La Quinta Ca, USA.
27. Jones R., Huang P. and Peng D., (2016) Crack growth from naturally occurring material discontinuities under constant amplitude and operational loads, International Journal of Fatigue, 91 pp. 434-444.
28. Molent L., Jones R (2016) The influence of cyclic stress intensity threshold on fatigue life scatter, International Journal of Fatigue, 82, pp. 748-756.
29. Jones R., Hu W. and Kinloch AJ., A convenient way to represent fatigue crack growth in structural adhesives, Fatigue and Fracture of Engineering Materials and Structures, 38, 4, pp. 379-391, 2015.
30. Jones R., Kinloch AJ., Michopoulos JG., Brunner AJ. and Phan N., (2017) Delamination growth in polymer-matrix fibre composites and the use of fracture mechanics data for material characterisation and life prediction, Composite Structures, 180, pp. 316-333.
31. Yao L., Alderliesten R., Jones R., Kinloch AJ., (2018) Delamination Fatigue Growth in Polymer-Matrix Fibre Composites: A Methodology for Determining the Design and Lifing Allowables, Composite Structures, 96, pp. 8-20.
32. Jones R, Steltzer S., Brunner A.J., Mode I, II and mixed mode I/II delamination growth in composites, Composite Structures, (2014), Composite Structures, 110 (2014), pp. 317-324.
33. Jones R, Pitt S., Brunner AJ., Hui D, Fatigue crack growth in nano-composites, Composite Structures, 99, 2013, pp. 375-379.
34. Jones R., Huang P. Peng D., Practical computational fracture mechanics for aircraft structural integrity, Chapter 4, pp. 67-128, Aircraft Sustainment and Repair, Edited by R. Jones, N. Matthews, AA. Baker and V. Champagne Jr., Butterworth-Heinemann Press, 2018, ISBN 9780081005408.
35. Walliker A., Progress report on DSTO intergranular corrosion-Fatigue interaction coupon test program, DSTO MI-9-3817, 29-11-2013.
36. Jones, R., Lo, M., Peng, D., Bowler, A., Dorman, M., Janardhana, M., Iyyer, NS., A study into the interaction of intergranular cracking and cracking at a fastener hole, Meccanica, 2015, vol. 50, issue 2, pp.517-532.
37. Peng, D., R. Jones, M. Lo, A. Bowler, G. Brick, M. Janardhana, D. Edwards, Crack growth at fastener holes containing intergranular cracking, Engineering Fracture Mechanics, 2015, vol. 137, pp. 79-87
38. Lo M., Jones R., Bowler A., Dorman M., and Edwards D., Crack growth at fastener holes containing intergranular cracking, Fatigue and Fracture of Engineering Materials and Structures, (2017) 40, 10, pp. 1664-1675.
39. Loader C., Goudie D., Salagaras M., J Underwood and A. Walliker, RAAF AP-3C Interaction between Intergranular Corrosion and Fatigue, DSTO Technical Report, DSTO-TR-3408, December 2014.
40. Barter SA., Molent L. and Wanhill RH. (2018) Typical fatigue-initiating discontinuities in metallic aircraft structures, Chapter 3, pp. 41-66, Aircraft Sustainment and Repair, Edited by R. Jones, N. Matthews, AA. Baker and V. Champagne Jr., Butterworth-Heinemann Press, 2018, ISBN 9780081005408.
41. Jones R. and Tamboli D., Implications of the lead crack philosophy and the role of short cracks in combat aircraft, Engineering Failure Analysis, 29, 2013, pp.149-166.
42. Peng D., Jones R., Sing RRK., Berto F., McMillan AJ., (2018) On the interaction between corrosion and fatigue which determines the remaining life of steel bridges, Fatigue & Fracture of Engineering Materials & Structures, 41, 2, pp. 314-322.
43. Jones R., Hui D., Analysis, design and assessment of composite repairs to operational aircraft, Chapter 8, pp. 325-456, Aircraft Sustainment and Repair, Edited by R. Jones, N. Matthews, AA. Baker and V. Champagne Jr., Butterworth-Heinemann Press, 2018, ISBN 9780081005408.
44. Jones R., Matthews N., Peng D., Phan N. and Nguyen T., Applications of SPD to enhance the structural integrity of corroded airframes, Chapter 16, pp. 863-906, Aircraft Sustainment and Repair, Edited by R.

Jones, N. Matthews, AA. Baker and V. Champagne Jr., Elsevier Butterworth-Heinemann Press, 2018, ISBN 9780081005408.

45. Wanhill RH., Environmental fatigue crack propagation in medium strength titanium sheet alloys, Enginming Fracture Mechanics, 1974, Vol. 6, pp. 681-697.
46. Kim S., Burns JT., Gangloff RP., Fatigue crack formation and growth from localized corrosion in Al-Zn-Mg-Cu, Engineering Fracture Mechanics 76 (2009) 651-667.
47. Jones, R., Lo, M., Peng, D., Bowler, A., Dorman, M., Janardhana, M., Iyyer, NS., A study into the interaction of intergranular cracking and cracking at a fastener hole, Meccanica, 2015, vol. 50, issue 2, pp.517-532.
48. Baker A. and Jones R., Bonded Repair of Aircraft Structure, Martinus Nijhoff Publishers, The Hague, 1988.
49. Jones R., Peng D., Matthews N. and Orchowski N., (2017) A study into the ability of SPD to restore the buckling strength and modes of rib stiffened panels with simulated stress corrosion cracks, International Journal of Structural Integrity, 8, 1, pp. 63-78.
50. Forman, RG, Mettu SR., Behavior of surface and corner cracks subjected to tensile and bending loads in Ti-6Al-4V alloy. In: Fracture Mechanics: 22nd Symposium, Vol. 1 (Eds H.A. Ernst, A. Saxena, D.L. McDowell), ASTM STP 1131, American Society for Testing and Materials, Philadelphia; 1992. pp.519-546.
51. Jones, R., Molent, L., and Walker, K., Fatigue crack growth in a diverse range of materials, International Journal of Fatigue, vol. 40, pp 43-50.
52. Horstemeyer MF., Farkas D., Kim S., Tang T., Potirniche G., Nanostructurally small cracks (NSC): A review on atomistic modeling of fatigue. International Journal of Fatigue, 32 (2010), pp. 1473-1502.
53. Jones R., Singh Raman RK., McMillan AJ., (2018) Crack growth: Does microstructure play a role? Engineering Fracture Mechanics, 187, pp. 190-210.
54. ASTM standard E647-13a Standard test method for measurement of fatigue crack growth rates, ASTM International, 2013。
55. Suresh, S., Ritchie, R.O., Propagation of short cracks, International Metals Reviews, 1984, vol. 29, issue 6, pp.445-76.